New Journal of Physics
The open access journal at the forefront of physics

Deutsche Physikalische Gesellschaft DPG
IOP Institute of Physics

Published in partnership with: Deutsche Physikalische Gesellschaft and the Institute of Physics

CrossMark

OPEN ACCESS

RECEIVED
17 April 2017

REVISED
17 June 2017

ACCEPTED FOR PUBLICATION
13 July 2017

PUBLISHED
4 October 2017

PAPER

Recovery time after localized perturbations in complex dynamical networks

Chiranjit Mitra[1,2], **Tim Kittel**[1,2], **Anshul Choudhary**[3], **Jürgen Kurths**[1,2] **and Reik V Donner**[1]

[1] Research Domain IV—Transdisciplinary Concepts & Methods, Potsdam Institute for Climate Impact Research, D-14473 Potsdam, Germany
[2] Department of Physics, Humboldt University of Berlin, D-12489 Berlin, Germany
[3] Theoretical Physics/Complex Systems, ICBM, Carl-von-Ossietzky University of Oldenburg, D-26111 Oldenburg, Germany

E-mail: chiranjit.mitra@pik-potsdam.de

Keywords: complex systems, nonlinear dynamics, networked dynamical systems, synchronization, transient stability against shocks, dynamical timescales

Abstract

Maintaining the synchronous motion of dynamical systems interacting on complex networks is often critical to their functionality. However, real-world networked dynamical systems operating synchronously are prone to random perturbations driving the system to arbitrary states within the corresponding basin of attraction, thereby leading to epochs of desynchronized dynamics with *a priori* unknown durations. Thus, it is highly relevant to have an estimate of the duration of such transient phases before the system returns to synchrony, following a random perturbation to the dynamical state of any particular node of the network. We address this issue here by proposing the framework of *single-node recovery time* (SNRT) which provides an estimate of the relative time scales underlying the transient dynamics of the nodes of a network during its restoration to synchrony. We utilize this in differentiating the particularly *slow* nodes of the network from the relatively *fast* nodes, thus identifying the critical nodes which when perturbed lead to significantly enlarged recovery time of the system before resuming synchronized operation. Further, we reveal explicit relationships between the SNRT values of a network, and its *global relaxation time* when starting all the nodes from random initial conditions. Earlier work on relaxation time generally focused on investigating its dependence on macroscopic topological properties of the respective network. However, we employ the proposed concept for deducing microscopic relationships between topological features of nodes and their respective SNRT values. The framework of SNRT is further extended to a measure of resilience of the different nodes of a networked dynamical system. We demonstrate the potential of SNRT in networks of Rössler oscillators on paradigmatic topologies and a model of the power grid of the United Kingdom with second-order Kuramoto-type nodal dynamics illustrating the conceivable practical applicability of the proposed concept.

1. Introduction

The abundance of dynamical systems involving large collections of individual entities interacting with each other on complex networks can hardly be further exaggerated [1–6]. Such networked dynamical systems often exhibit a multitude of stable states, whereby sustained operation of the system in the desired state is of central importance. The desired operational state (DOS) in such systems is commonly associated with the synchronized motion of the dynamical components coupled on their networked architecture [7, 8]. 'Permissible' and 'impermissible' random perturbations (according to the terminology used by Menck *et al* [9]) often disrupt the functionality of coupled dynamical systems operating in the synchronized state, driving them away either to an arbitrary state still inside the basin of attraction of the synchronized state, or to an altogether different dynamical regime. The former situation arising on account of 'permissible' perturbations, leads to arbitrary durations of

desynchronized dynamics before the system regains synchronous motion. On the other hand, 'impermissible' perturbations permanently forbid the return of the system to the synchronized state, unless again affected by an appropriate external perturbation.

The stability of the synchronized state against the aforementioned perturbations is critical in the operation of many real-world networked dynamical systems such as ecosystems, power grids, the human brain, etc [10]. Subsequently, the influence of topological features on network synchronizability and the stability of the synchronized state has been well-investigated [7, 11]. In this context, significant developments constitute the master stability function (MSF) [12], basin stability (BS) [9] and its extensions to single-node BS [8], multiple-node BS [10], and survivability [13]. On the contrary, the issue of recovery time (RT) of complex dynamical networks following a random perturbation, which is a measure of how quickly the network relaxes back to the DOS (e.g., a synchronized state) after being perturbed from the same, has received considerably less attention and is currently under active investigation [14–25]. However, this is an important problem concerning dynamical robustness of complex networks, i.e., the ability of a network to restore its dynamical activity to the DOS when its components are subject to random perturbations. For example, the loss of synchrony in engineered systems such as power grids can lead to large-scale power blackouts [8]. In biological systems such as the human brain, it can impede cognitive functions such as information transfer [26] and memory [27]. Thus, quickly restoring synchrony following desynchronizing perturbations is crucial in such coupled dynamical systems. Consequently, it is highly desirable to have an estimate of the RT of the system to the desired stable regime, following a perturbation to a particular node of the network (otherwise operating in the DOS). This creates the possibility of identifying (and safeguarding) specific nodes which when perturbed lead to a particularly large RT of the system. In this regard, we propose here the framework of *single-node recovery time* (SNRT) addressing the aforementioned issue. We reserve a formal definition of SNRT to section 2.3.

SNRT of a node under investigation relates to the time taken by the system operating in the DOS (e.g., a synchronized state) to return to the same, following a random perturbation to the dynamical state of the respective node. The framework of SNRT provides information on the different relative time scales underlying the transient dynamics of the respective nodes of the network during its restoration to the DOS. This can be utilized in revealing the particularly *slow* nodes of the network in contrast to the relatively *fast* ones, leading to the identification of the vulnerable nodes which when perturbed significantly elevate the RT of the whole system. Further, this can provide an insight into the *global relaxation time* (GRT) of the network to the DOS, when starting all its nodes from arbitrary initial conditions. We provide a formal definition of GRT in section 2.4. The GRT is referred to as the *global synchronization time* when the synchronized state is the DOS of the network.

Previously, the dependence of synchronization time on various macroscopic topological properties of the corresponding networks has been investigated. For example, Grabow *et al* [22] have shown that, largely insensitive to the type of oscillators (phase, multi-dimensional, neural), their intrinsic dynamics (periodic, chaotic) and their coupling schemes (phase-difference, diffusive, pulse-like), networks with a fixed average path length consistently synchronize slowest in the small-world regime. This is a rather unexpected phenomenon given that small-world topology has been suggested to facilitate network synchronization at weaker coupling strengths (than for analogous, appropriately normalized globally coupled systems) [28–30] as well as being more robust to random perturbations [9]. Also, the MSF approach [12] has been extended by Grabow *et al* [23] to provide analytical predictions for the asymptotic synchronization times, which is, however, locally restrictive to small perturbations. Further, the dependence of synchronization time on various macroscopic topological features such as the average path length, global clustering coefficient, etc has been systematically studied. In this context, the framework of SNRT introduced in this work is capable of providing a microscopic view on the response to arbitrary perturbations of individual nodes as well as exploring relationships between various topological features of the nodes and their respective SNRT values.

Finally, we advance on the framework of SNRT for quantifying the resilience of networked dynamical systems [31]. Resilience of a given dynamical system has been defined in at least two different ways, namely, *engineering resilience* and *ecological resilience* [32]. Engineering resilience (according to Pimm [33]) of a dynamical system characterizes its resistance to disturbance and speed of return to its equilibrium, following a perturbation [32, 34, 35]. It implicitly assumes global stability, i.e., the existence of only one equilibrium state, or, if other operating states exist, they should be avoided by applying safeguards [32, 34, 35]. On the other hand, ecological resilience [36] presumes the existence of multiple stable states and the tolerance of the system to disturbances that facilitate transitions among the stable states [32, 34, 35]. In this case, resilience of the system is measured by its capacity to remain in the same basin of attraction in the face of random perturbations [32, 34, 35].

Ecological resilience of the multiple stable states of a system relates to the volume and geometry of their respective basins of attraction [9, 35]. In this context, Mitra *et al* [35] recently reconsidered the concept of ecological resilience and its three crucial aspects of 'latitude' (L), 'resistance' (R) and 'precariousness' (Pr) [36]. They redefined L, R and Pr in a rigorous dynamical systems context and utilized this as a foundation for characterizing multistability and proposing the quantifier of *integral stability* [35]. Besides its extension to quantifying multistability, the

framework of ecological resilience has generated widespread interest (see [37] and references therein). On the other hand, the facet of engineering resilience, perhaps on account of its restrictive scope to globally stable systems has received considerably less attention. However, it is equally crucial to know how long does a system operating in its desired stable state take to retain functionality in the respective dynamical state, following a random perturbation. As mentioned earlier, networked dynamical systems often exhibit multiple stable states, such as the coexistence of synchronized and desynchronized dynamical regimes, which is a notable example of bistable behaviour [10]. Thus, we extend here the traditional scope of engineering resilience to quantifying the resilience of the DOS (e.g., the synchronized state) in such multistable coupled dynamical systems. More precisely, we relate the engineering resilience of each node of a networked dynamical system (for the DOS) to the SNRT of the corresponding node such that a node with a lower value of SNRT is considered more resilient and vice versa. Thus, the proposed architecture of engineering resilience complements the existing framework of ecological resilience in characterizing the overall resilience of networked dynamical systems.

This paper is further organized as follows: in section 2, we outline the general methodology for calculating SNRT values for a given networked dynamical system. In section 3, we illustrate applications of SNRT to networks of Rössler oscillators and a model of the power grid of the United Kingdom with second-order Kuramoto-type nodal dynamics. Finally, we present the conclusions of our work in section 4.

2. Methods

2.1. Preliminaries

Consider a network of N oscillators (nodes) where the intrinsic dynamics of the ith oscillator (represented by the d-dimensional state vector $\mathbf{x}_i(t) = (x_i^1, x_i^2, \ldots, x_i^d)^{\mathrm{T}}$) is described by $\dot{\mathbf{x}}_i = \mathbf{F}_i(\mathbf{x}_i)$, where $\mathbf{x}_i \in \mathbb{R}^d$; $\mathbf{F}_i : \mathbb{R}^d \to \mathbb{R}^d$, $\mathbf{F}_i = (F_i^1(\mathbf{x}_i), F_i^2(\mathbf{x}_i), \ldots, F_i^d(\mathbf{x}_i))^{\mathrm{T}}$; $i = 1, 2, \ldots, N$. The dynamical equations of the networked system read

$$\dot{\mathbf{x}}_i = \mathbf{F}_i(\mathbf{x}_i) + \epsilon \sum_{j=1}^{N} A_{ij} \mathbf{H}_{ij}(\mathbf{x}_i, \mathbf{x}_j), \tag{1}$$

where ϵ is the overall coupling strength, $\mathbf{A}$ is the adjacency matrix which captures the interactions between the nodes such that $A_{ij} \neq 0$ if node j influences node i and $\mathbf{H}_{ij} : \mathbb{R}^d \times \mathbb{R}^d \to \mathbb{R}^d$ is an arbitrary coupling function from nodes j to i. For the illustrations in this paper (section 3), we consider identical nodal dynamics ($\mathbf{F}_i = \mathbf{F}\ \forall i$), symmetric adjacency matrices ($A_{ij} = A_{ji} = 1$ if nodes i and j are connected and $A_{ij} = A_{ji} = 0$ otherwise) and identical coupling functions ($\mathbf{H}_{ij} = \mathbf{H}\ \forall i, j$).

We assume that the DOS is an attractor of the system that we denote by $\mathcal{A}$ with the corresponding basin of attraction $\mathcal{B}(\mathcal{A})$. We usually denote a trajectory on $\mathcal{A}$ by $\tilde{\mathbf{x}}(t)$.

2.2. Regularized reaching time

For a trajectory initiated from $\mathbf{x}(0) = (\mathbf{x}_1(0), \mathbf{x}_2(0), \ldots, \mathbf{x}_N(0))^{\mathrm{T}} \in \mathcal{B}(\mathcal{A})$, the attractor is usually reached asymptotically. This implies that the associated reaching time is not finite, thus posing a problem in its measurement. A way to address this problem is regularization of the time variable [25]. We now discuss the framework of *regularized reaching time* proposed by Kittel *et al* [25] and then resort to the same in dealing with the above issue.

The distance of a state at time t on a trajectory initiated from $\mathbf{x}(0)$, to the desired attractor is given by,

$$d(\mathbf{x}(t, \mathbf{x}(0)), \mathcal{A}) = \inf\{\|\mathbf{x}(t, \mathbf{x}(0)) - \mathbf{x}'\| : \mathbf{x}' \in \mathcal{A}\},$$

where $\mathbf{x}(t, \mathbf{x}(0))$ represents the state of the system after a time t has elapsed. The last-entry time for the corresponding trajectory to enter a δ-neighbourhood around the desired attractor $\mathcal{A}$ is given by

$$t_{\mathrm{L}}(\mathbf{x}(0), \delta) = \inf\{T : d(\mathbf{x}(t, \mathbf{x}(0)), \mathcal{A}) < \delta, \forall t \geqslant T\},$$

where $\delta \to 0$ leads to the aforementioned divergence.

Kittel *et al* [25] argued that even though the actual reaching times diverge for the respective trajectories, their differences actually converge. Subsequently, they proposed the *regularized reaching time* $T_{\mathrm{RR}}(\mathbf{x}(0))$ for any trajectory (starting from $\mathbf{x}(0)$) as the difference between the last-entry times along the respective trajectory and a reference trajectory (starting from $\mathbf{x}_{\mathrm{ref}}$), for a given $\delta > 0$. This can be interpreted as the additional time the trajectory starting from $\mathbf{x}(0)$ needs to arrive in the vicinity of the desired attractor, after the reference trajectory starting from $\mathbf{x}_{\mathrm{ref}}$ has reached it. Thus,

$$T_{\mathrm{RR}}(\mathbf{x}(0)) = \lim_{\delta \to 0}(t_{\mathrm{L}}(\mathbf{x}(0), \delta) - t_{\mathrm{L}}(\mathbf{x}_{\mathrm{ref}}, \delta)). \tag{2}$$

A positive or negative value of $T_{\mathrm{RR}}(\mathbf{x}(0))$ indicates that the considered trajectory arrives by this value *later* or *earlier* than the reference trajectory, respectively. This allows the distinction between *slower* and *faster* trajectories of the system during their return to the desired attractor (see Kittel *et al* [25] for further details on T_{RR}).

2.3. Single-node recovery time (SNRT)

In the following, we outline the general methodology for calculating SNRT values for all nodes of any networked dynamical system. We assume that the networked dynamical system of equation (1) is in its DOS $\tilde{\mathbf{x}}(t)$. Now, consider a 'permissible' random perturbation $\Delta\mathbf{x}_i$ to the dynamical state of the ith oscillator of the network. The system (otherwise functioning in its DOS) is pushed to a perturbed state $\mathbf{x}_{\Delta i} = (\tilde{\mathbf{x}}_1, \tilde{\mathbf{x}}_2, \ldots, \tilde{\mathbf{x}}_i + \Delta\mathbf{x}_i, \ldots, \tilde{\mathbf{x}}_N)^{\mathrm{T}}$. The perturbed state (on account of the perturbation being 'permissible') remains in the basin of attraction $\mathcal{B}(\mathcal{A})$ of the DOS because we chose $\mathbf{x}_{\Delta i}$ to be permissible, thus ensuring the system's return to the same. We then define the SNRT of the ith oscillator as,

$$\langle T_R^1(i)\rangle = \frac{\int_{P_i(\mathcal{B}(\mathcal{A}))} \rho_i(\mathbf{x}_{\Delta i})\, T_{\mathrm{RR}}(\mathbf{x}_{\Delta i})\, \mathrm{d}\Delta\mathbf{x}_i}{\int_{P_i(\mathcal{B}(\mathcal{A}))} \rho_i(\mathbf{x}_{\Delta i})\, \mathrm{d}\Delta\mathbf{x}_i}, \tag{3}$$

where P_i is the projector into the subspace of the ith oscillator, i.e., $P_i(\mathbf{x}) = \mathbf{x}_i$. $\rho_i(\mathbf{x}_{\Delta i})$ is the density of 'permissible' perturbed states in state space that the ith oscillator may be pushed to even via large perturbations with $\int \rho_i(\mathbf{x}_{\Delta i})\mathrm{d}\Delta\mathbf{x}_i = 1$, where this integral is performed over the subspace of the ith oscillator. The integrals in the numerator and denominator of equation (3) are performed over the basin of attraction of the DOS (i.e., $\mathbf{x}_{\Delta i} \in \mathcal{B}(\mathcal{A})$). Thus, the SNRT of the ith oscillator $\langle T_R^1(i)\rangle$ corresponds to the mean regularized reaching time of the system to the DOS, after a random 'permissible' perturbation hits the respective oscillator.

Equation (2) demands the choice of a reference initial condition $\mathbf{x}_{\mathrm{ref}} \in \mathcal{B}(\mathcal{A})$ that needs to be kept fixed for all single-node perturbations to allow comparability between SNRT values of the different nodes of the network. However, different choices of $\mathbf{x}_{\mathrm{ref}}$ (as long as we do not choose it on $\mathcal{A}$) simply lead to a shift of all $\langle T_R^1(i)\rangle$ values by a constant only [25]. Although not posing a serious problem, this methodology of choosing $\mathbf{x}_{\mathrm{ref}}$ leaves an element of arbitrariness. As we seek to utilize the $\langle T_R^1\rangle$ values in estimating the duration by which a particular node of the network returns *faster* or *slower* than another, this naturally leads to the condition demanding the lowest $\langle T_R^1(i)\rangle$ value to be 0,

$$\min_i(\langle T_R^1(i)\rangle) = \langle T_R^1\rangle_{\min} = 0. \tag{4}$$

Using this equation, we can fix $\mathbf{x}_{\mathrm{ref}}$ implicitly instead of explicitly specifying it. We denote the node (or one representative if there might be more) with $\langle T_R^1(i)\rangle = 0$ by i_{ref}. The resulting values of $\langle T_R^1\rangle$ now represent differences in time by which nodes of the network return *slower* than the reference node i_{ref}. As opposed to arbitrarily choosing $\mathbf{x}_{\mathrm{ref}}$, thereby resulting in negative T_{RR} values (which is counter-intuitive when measuring time), the above choice of $\mathbf{x}_{\mathrm{ref}}$ ensures non-negativity of $\langle T_R^1(i)\rangle$ values, besides eliminating the arbitrariness associated with the choice of $\mathbf{x}_{\mathrm{ref}}$. Further details on the choice of the reference trajectory are provided in appendix A.

We now present an algorithm for estimating the SNRT of the ith oscillator/node of a network (modelled using equation (1)):

(i) Identify the DOS of the network. This state often corresponds to the synchronized dynamics of the oscillators coupled on the network.

(ii) When the attractor corresponding to the DOS $\mathcal{A}$ is not a fixed point, choose P (>1) different points on the attractor. Otherwise, choose $P = 1$.

(iii) For a particular value of p $(p = 1, 2, \ldots, P)$, initiate the system from the DOS corresponding to the pth point on $\mathcal{A}$. Then, perturb the ith oscillator by drawing I_C randomly distributed (according to $\rho_i(\mathbf{x}_{\Delta i})$) initial conditions $\mathbf{x}_{\Delta i}^p(j = 1, 2, \ldots, I_C)$ from inside the basin of attraction of the DOS. For the results described in this paper, we assume a uniform distribution of $\rho_i(\mathbf{x}_{\Delta i})$.

(iv) For a fixed value of $\delta > 0$, calculate the last-entry time $t_{\mathrm{L}}(\mathbf{x}_{\Delta i}^p(j), \delta)$ of the system for the jth initial condition.

(v) Estimate the SNRT of the ith oscillator $(T_R^1(i, p))$ for the pth point on the attractor as,

$$\hat{T}_R^1(i, p) = \frac{\sum_{j=1}^{I_C} t_{\mathrm{L}}(\mathbf{x}_{\Delta i}^p(j), \delta)}{I_C}, \tag{5}$$

and then average over p to obtain,

$$\langle T_R^1(i)\rangle = \frac{1}{P}\sum_{p=1}^{P} \hat{T}_R^1(i, p). \tag{6}$$

(vi) Finally, we identify the node i_{ref} with the minimum $\langle T_R^1 \rangle$ value (as computed above for all nodes) $\langle T_R^1 \rangle_{\min}$ and subtract this value from the $\langle T_R^1(i) \rangle$ of the ith oscillator computed above, thus yielding the SNRT value of the respective oscillator.

The parameters P, I_C and δ of the above algorithm have to be selected prior to its implementation. The actual values should be chosen according to the specifics of the system under investigation, as also illustrated with the different applications presented in this paper (section 3). It is conclusive however, that higher values of P and I_C yield better estimates of $\langle T_R^1(i) \rangle$.

As mentioned earlier, this concept of SNRT can be utilized in identifying the *slow* and *fast* nodes/sub-components of networked dynamical systems. Also, the proposed machinery can be used in revealing systematic relationships between SNRT values of different nodes and their respective topological features. Further, it can be extended to a measure of (engineering) resilience of the different nodes of a networked dynamical system (see section 2.6) and thereby utilized in identifying the particularly vulnerable nodes of the network as well as the more resilient ones. Subsequently, this framework of SNRT can be potentially relevant in selecting specific nodes to be safeguarded from external perturbations. We now define the GRT of a network, which relates to the overall time scale of the dynamics of a network during its relaxation to the DOS.

2.4. Global relaxation time (GRT)

Starting all nodes of a networked dynamical system from random initial conditions inside the basin of attraction of the desired attractor involves a transient time before the system reaches the associated attractor. We refer to the duration of this transient regime as the *relaxation time* of the system for the respective initial state. We estimate the GRT $\langle T_R \rangle$ of a network as follows:

(i) Draw I_C random initial conditions from inside the basin of attraction of the DOS. The jth initial condition can be written as $\mathbf{x}(j) = (\mathbf{x}^1, \mathbf{x}^2, \ldots, \mathbf{x}^N)^{\mathrm{T}}$ where $j = 1, 2, \ldots, I_C$. Note, that the value of I_C chosen for computing the GRT can be different from the one chosen for calculating SNRT above (section 2.3).

(ii) For the jth initial condition, calculate the last-entry time $t_{\mathrm{L}}(\mathbf{x}(j), \delta)$ of the system with the same value of δ as chosen for computing SNRT (section 2.3).

(iii) Calculate the GRT of the network as,

$$\langle T_R \rangle = \frac{1}{I_C} \sum_{j=1}^{I_C} t_{\mathrm{L}}(\mathbf{x}(j), \delta). \tag{7}$$

(iv) Finally, subtract the value of $\langle T_R^1 \rangle_{\min}$ (obtained in section 2.3) from the $\langle T_R \rangle$ computed above in obtaining the GRT of the network.

When the DOS of the network is a synchronized state, its GRT is referred to as the *global synchronization time* of the system.

The GRT of a network is useful for quantifying the expected transient time to reach the DOS, when starting the system from a random initial condition. In section 3, we will illustrate the relationship between SNRT values and the GRT of a network for different systems.

In order to avoid terminological confusion, we explicitly distinguish between the usage of *recovery*, *reaching* and *relaxation* time. We use the term *recovery* with reference to the time taken by the system to recover from a perturbation and resume operation in the DOS. On the other hand, when initiating all the nodes of the system from arbitrary conditions, the term *relaxation* is used with reference to the time before the system relaxes to the DOS. It is the difference between the relaxation times of a trajectory starting from a particular initial condition and that of a reference trajectory, which is termed as the regularized *reaching* time for the respective initial condition.

It should be noted that the situation following a perturbation may also be viewed as the system starting from a particular initial condition (corresponding to the perturbed state) and subsequently, relaxing to the respective attractor. However, we want to specifically distinguish between relaxation following a perturbation as a process of *recovery*, and the traditional formalism of *relaxation* of the system when starting the entire network from random initial conditions. Subsequently, we seek to utilize the above terminology in order to maintain this distinction during the course of this work.

2.5. Single-node basin stability (SNBS)

The BS of a particular attractor relates the volume of its basin of attraction to the likelihood of returning to the same attractor in the face of random perturbations [8–10]. More precisely, the BS of a particular attractor is

defined as the fraction of the volume of the state space belonging to the basin of attraction of the respective attractor [8–10]. In practice, BS of any particular attractor is estimated using a numerical Monte Carlo procedure by drawing random initial states from a chosen subset of the entire state space, simulating the associated trajectories, and calculating the fraction of trajectories that approach the respective attractor [8–10]. As mentioned earlier, the ecological resilience of a stable state is (among other properties) determined by the size and shape of its basin of attraction, and is therefore closely related to its BS.

BS has been further extended to the framework of SNBS [8, 10]. SNBS $\langle S_B^1 \rangle$ of a node under investigation corresponds to the probability of the network (operating in the DOS) to return to the DOS, after that particular node has been hit by a non-infinitesimal perturbation [8, 10]. We refer to Mitra *et al* [10] for the general methodology used throughout this paper for estimating SNBS values for any networked dynamical system.

2.6. Engineering resilience

SNBS is a measure related to the ecological resilience of a node subjected to a random perturbation (when the entire network was functioning in the DOS prior to the disturbance). The time elapsed before the network returns to its DOS, following a 'permissible' random perturbation to a particular node determines the engineering resilience of the respective node. We recommend incorporating the engineering resilience of a node (besides its ecological resilience as characterized by its SNBS value) quantified as being inversely related to its SNRT value, in measuring the overall resilience of the respective node. For example, it may be possible that two nodes of a networked dynamical system have very similar values of SNBS. However, the SNRT values of the respective nodes may differ significantly (as we shall illustrate using examples in section 3). In such a situation, the new framework of SNRT should complement that of SNBS in appropriately assessing the resilience of the respective nodes of a network.

3. Examples

We shall now illustrate applications of SNRT to various networked dynamical systems. Here, we specifically apply the framework to networks of oscillators with continuous time dynamics (equation (1)) exhibiting bistability on account of coexisting synchronized and desynchronized regimes, where the former is considered as the DOS of the system. However, the framework is generally applicable to (continuous or discrete time) networked dynamical systems with multiple coexisting states as well. It should be noted that the values of the measures for the different networks/examples studied in this work are not directly comparable. Also, the algorithmic parameters for each application have been chosen according to the specific system under investigation.

3.1. Deterministic scale-free (DSF) network of Rössler oscillators

We first consider a network of N identical Rössler oscillators [38], with diffusive coupling in the x^2-variable between two coupled nodes such that the full dynamical equations of node i (in analogy with equation (1)) read

$$\begin{aligned} \dot{x}_i^1 &= -x_i^2 - x_i^3, \\ \dot{x}_i^2 &= x_i^2 + a x_i^2 + \epsilon \sum_{j=1}^{N} A_{ij}(x_j^2 - x_i^2), \\ \dot{x}_i^3 &= b + x_i^3(x_i^1 - c). \end{aligned} \tag{8}$$

We use the parameter values of $a = b = 0.2$ and $c = 7.0$ for which the intrinsic dynamics of each uncoupled Rössler oscillator is chaotic.

As a specific network topology, we use an undirected DSF network [39]. For the simulations carried out in this section, we specifically generate a DSF network developed over three generations and hence, comprising $N = 81$ nodes (figure 1). We refer the reader to appendix B for further details on the DSF network model.

We consider the completely synchronized state as the DOS of the network, which corresponds to all oscillators following the same trajectory. Further, we choose $\epsilon = 0.8$ for which the completely synchronized state in Rössler oscillators diffusively coupled via the x^2-variable is stable (see [40] for further details on the calculation of the stability interval) and set $\delta = 10^{-4}$ [4] for estimating the SNRT ($\langle T_R^1 \rangle$) values, using the procedure described in section 2.3.

[4] We suggest choosing a value of δ depending upon the system of interest. This choice should be made to ensure that the system comes sufficiently close to the desired attractor $\mathcal{A}$ as well as being computationally efficient. For example, we choose a value of $\delta = 10^{-4}$ for the deterministic scale-free network, whereas $\delta = 10^{-6}$ for the random scale-free network. This is because in the former case, the system generally takes a longer time to enter the δ-environment around $\mathcal{A}$. For a further discussion on the estimation of T_{RR}, we refer the reader to [25].

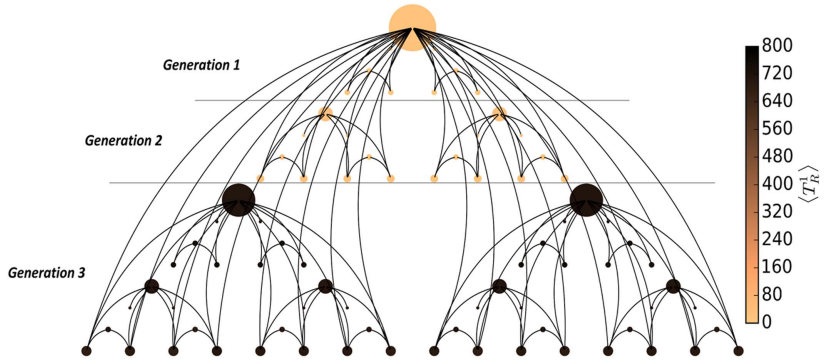

Figure 1. Network topology of the undirected deterministic scale-free network of $N = 81$ identical Rössler oscillators. The size of each node is proportional to its degree and the colour indicates the $\langle T_R^1 \rangle$ value of the respective node.

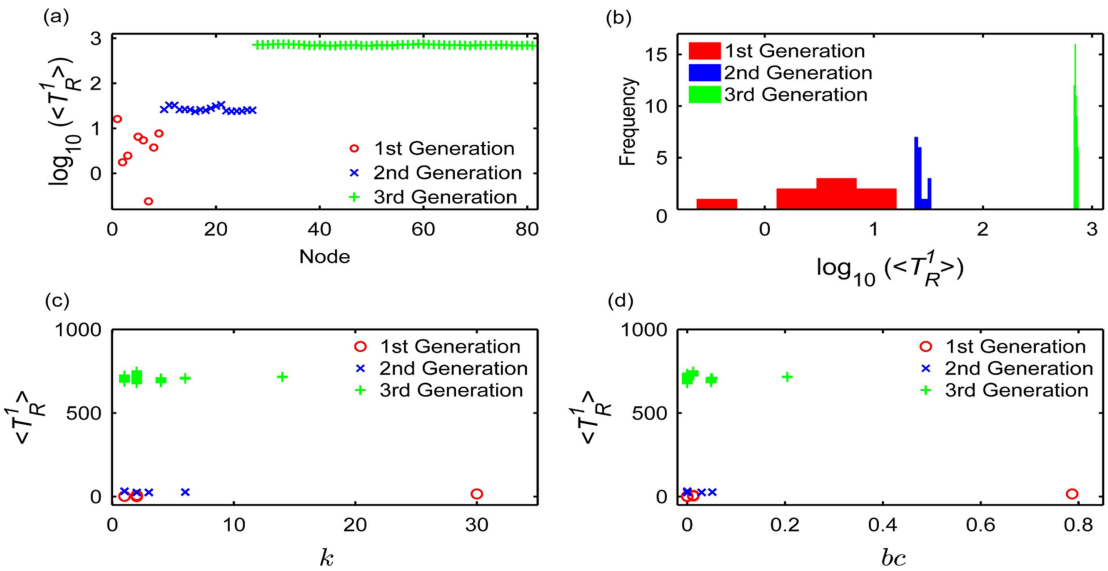

Figure 2. (a) SNRT $\langle T_R^1 \rangle$ (on $\log_{10}$ scale) of the nodes of the three generations of the undirected DSF network of N identical Rössler oscillators (equation (8)). The first nine nodes comprise the 1st generation, the next 18 nodes the 2nd generation and the final 54 nodes the 3rd generation. Node 4 having the minimum SNRT value $\langle T_R^1(4) \rangle = 0$ of the network (implying divergence of $\log_{10}(\langle T_R^1(4) \rangle)$) has not been shown in the plot. Note that the $\langle T_R^1 \rangle$ values of the nine nodes comprising the 1st generation are actually between 0 and 17. However, as the $\langle T_R^1 \rangle$ values are presented on a $\log_{10}$ scale, they appear to be much more dispersed than the $\log_{10}(\langle T_R^1 \rangle)$ values of the nodes in the other two generations. However, the $\langle T_R^1 \rangle$ values of the nodes in all the three generations actually have similar variations. (b) Histogram of $\log_{10}(\langle T_R^1 \rangle)$ of the nodes. (c), (d) Relationship of $\langle T_R^1 \rangle$ with (c) degree (k) and (d) betweenness centrality (bc) of the nodes.

We calculate and present the individual $\langle T_R^1 \rangle$ (on $\log_{10}$ scale) values of the nodes in figure 2(a). Interestingly, the three generations of nodes split into three classes in terms of their $\langle T_R^1 \rangle$ values such that the lower the generation in the hierarchy, the higher is the SNRT of the individual nodes comprising it (as evident from the histogram in figure 2(b)).

We next compare these findings with two key topological features of the DSF network. The connectivity of a node i (for $i = 1, 2, \ldots, 81$) is described by its degree $k_i = \sum_j A_{ij}$ (where $\mathbf{A}$ is again the adjacency matrix of the respective network [6]). The betweenness centrality (bc_i) of a node i is related to the fraction of shortest paths between all pairs of nodes that pass through node i [6]. For an N-node network, the bc of each node may further be normalized by dividing by the number of node pairs $\left(\text{i.e.}, \binom{N}{2}\right)$, obtaining a value between 0 and 1. Thus, $bc_i = \frac{2}{N(N-1)} \sum_{j \neq k \neq i} \frac{\sigma_{j,k}^i}{\sigma_{j,k}}$ where $\sigma_{j,k}$ is the total number of shortest paths from nodes j to k and $\sigma_{j,k}^i$ is the number of such shortest paths which pass through node i [6].

Figures 2(c), (d) shows the relationship of the $\log_{10}(\langle T_R^1 \rangle)$ values with the topological features of degree k and bc of the nodes, respectively. The $\langle T_R^1 \rangle$ values do not exhibit any marked relationship with these two characteristics. This is further illustrated by the correlation coefficient of -0.040 (-0.085) between $\langle T_R^1 \rangle$ and

$k\,(bc)$. We summarize our results in figure 1, which displays the network topology where the size of each node is proportional to the degree and the colour corresponds to the $\langle T_R^1 \rangle$ value of the respective node.

The nodes in the 3rd generation of the DSF network comprise its *slow* nodes. It is expected that the overall time scale of synchronization of a network should be governed by the node with the highest SNRT, i.e., the 'slowest' node of the system. The 'slowest' node of the DSF network has $\langle T_R^1 \rangle \approx 749.8$. We also computed the GRT $\langle T_R \rangle$ of the DSF network using the methodology described in section 2.4. We find $\langle T_R \rangle \approx 750.04$ being very close to the maximum $\langle T_R^1 \rangle$ value of the network. Thus, we conclude that the 'slowest' nodes of the DSF network indeed govern its overall time scale of synchronization. However, this result cannot be generalized to any arbitrary topology, as we will demonstrate in the following.

3.2. Random scale-free networks of Rössler oscillators

Next, we consider an ensemble of 100 random scale-free networks (generated using the classical Barabási–Albert (BA) model of growth and preferential attachment [41]) of $N = 81$ Rössler oscillators each, with the same parameter values as for the DSF network. We refer the reader to appendix C for further details on the BA network model. While the DSF network of $N = 81$ Rössler oscillators studied in section 3.1 had 130 edges, equivalently, an edge density of $\frac{130}{\binom{81}{2}} \approx 0.04$, the random scale-free networks generated using the classical BA model have edge densities of 0.049, i.e., 158 edges in each realization. This means that the BA random scale-free networks have 22.5% more edges than the DSF network considered earlier in section 3.1. Therefore, the results obtained for both topologies are not directly comparable quantitatively.

The distribution of SNBS $\langle S_B^1 \rangle$ values of the $N = 81$ nodes of the considered ensemble is presented in figure 3(a). Surprisingly, all nodes have similar and very high $\langle S_B^1 \rangle$ values. Similar results have been observed in a recent study on SNBS values in the DSF network of Rössler oscillators [10]. Figures 2 and 3 in [10] present the distribution of the $\langle S_B^1 \rangle$ values of the $N = 81$ nodes of the DSF network, considered in section 3.1 of this paper. Clearly, the $\langle S_B^1 \rangle$ values of all the nodes are very high (~0.95) as well as very similar. Likewise, figure 3(a) here illustrates the distribution of the $\langle S_B^1 \rangle$ values of all the nodes of the considered ensemble of BA random scale-free networks, which are again equally high (~0.95) and also quite similar for all nodes of the ensemble. These observations lead to two important conclusions. Firstly, the similar and rather high $\langle S_B^1 \rangle$ values indicate that the synchronized state in scale-free networks is generally very robust to perturbations affecting a single node of the system. Secondly, we observe that the presence or lack of a specific macroscopic (hierarchical) structure (as in the DSF network but not in its random counterpart) in the respective scale-free network does not affect the distribution of its $\langle S_B^1 \rangle$ values markedly. In contrast to the latter finding, we have already observed an influence of the hierarchical structure on $\langle T_R^1 \rangle$ for the DSF network (figure 2(a)). On this note, we shall further unfold dependences of $\langle T_R^1 \rangle$ values on different topological features of random scale-free networks.

The corresponding distribution of $\langle T_R^1 \rangle$ (for $\delta = 10^{-6}$ (see footnote 4)) of all nodes of the considered ensemble of random scale-free networks is shown in figure 3(b). As in the case of the DSF network, we next consider the mutual dependence between SNRT and the local topological characteristics of the network. For this purpose, we study the distribution of $\langle T_R^1 \rangle$ values of all nodes of the ensemble with respect to their degree and bc. We collect all nodes of the ensemble having a particular degree k and calculate the mean over the $\langle T_R^1 \rangle$ values of all these nodes which corresponds to the conditional mean $\langle\langle T_R^1 \rangle | k \rangle$. Similarly, we bin the bc values of all nodes of the ensemble and calculate the conditional mean $\langle\langle T_R^1 \rangle | bc \rangle$ over the $\langle T_R^1 \rangle$ values of all nodes belonging to the respective bin. Interestingly, the conditional mean values exhibit a strong linear dependency with respect to k and bc as illustrated in figures 3(c), (d). This is further underlined by correlation coefficients of 0.987 (0.991) of the conditional means with $k\,(bc)$. Thus, nodes with high k and bc, namely the hubs in the random scale-free network, can be classified as its *slow* nodes. Perturbations to a more central node of a scale-free network (operating in the synchronized state) can easily spread to other nodes of the network driving them further away from the synchronized state. As a result, a scale-free network operating in synchrony may take longer to resynchronize when its more central nodes are perturbed as opposed to less central ones. This observation is supported by the positive correlation between the conditional mean $\langle\langle T_R^1 \rangle | bc \rangle$ and bc. Further, given the strong linear relationship of the conditional mean SNRT with bc, a similar dependence for k is to be expected (and vice versa) since random scale-free networks generally exhibit a strong correlation between k and bc of their nodes [42]. However, the relationship of the conditional mean SNRT with k and bc being specifically linear is surprising and revealing the underlying reason requires further investigation. We emphasize that the observed relations are not specific to the relatively small network size. For example, we have obtained similar results (not shown) in an ensemble of 100 random BA scale-free networks, each comprising 243 Rössler oscillators constituting the nodal dynamics (with similar parameter values as above but for $\epsilon = 1.3$).

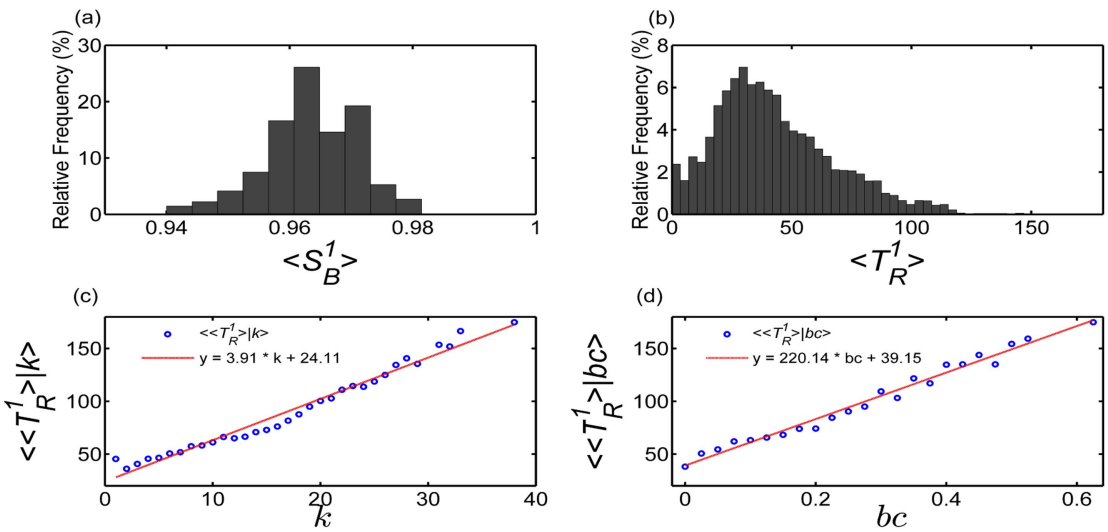

Figure 3. (a) Histogram of SNBS $\langle S_B^1 \rangle$ of all nodes of the considered ensemble of random scale-free networks. The relative frequencies (%) correspond to the percentage of nodes with $\langle S_B^1 \rangle$ values lying within the respective bin of the histogram. (b) Same for the $\langle T_R^1 \rangle$ values. (c), (d) Conditional means (blue circles) of $\langle T_R^1 \rangle$ with respect to (c) degree ($\langle\langle T_R^1 \rangle | k \rangle$) and (d) betweenness centrality ($\langle\langle T_R^1 \rangle | bc \rangle$) of the nodes. The red lines indicate linear fits to the conditional means.

We now calculate and present the GRT $\langle T_R \rangle$ of all members of the considered ensemble of random scale-free networks (figure 4(a), black circles). Interestingly, we observe that unlike for the DSF network, the overall time scale of synchronization in the different network realizations of its random counterpart differs markedly from the maximum SNRT (red crosses) of the respective realization. To further study this finding, for each network realization we compute the average of the $\langle T_R^1 \rangle$ values of all its $N = 81$ nodes and denote it by $\langle\langle T_R^1 \rangle\rangle$. Notably, the $\langle T_R \rangle$ value of every network realization appears closely related to $\langle\langle T_R^1 \rangle\rangle$ (blue crosses) as illustrated in figure 4(a). This is also corroborated by a correlation coefficient of 0.991 between $\langle T_R \rangle$ and $\langle\langle T_R^1 \rangle\rangle$.

Figure 4(b) shows the maximum $bc_{\max}$ of all nodes of each network realization and its relationship with the GRT $\langle T_R \rangle$ of the respective realization. As mentioned earlier, perturbing the node with $bc_{\max}$ in a scale-free network (operating in the synchronized state) may lead to a particularly large relaxation time to the synchronized state. Thus, the higher the maximum bc of a scale-free network, the higher is the GRT of the system, which is underlined by the positive correlation coefficient of 0.882 between $\langle T_R \rangle$ and $bc_{\max}$ in figure 4(b).

The average path length $\mathcal{L}$ of a network is defined as the mean value of the shortest path length between all possible pairs of vertices [6]. Thus, $\mathcal{L} = \frac{1}{N(N-1)} \sum_{i \neq j} \ell(i, j)$ where $\ell(i, j)$ is the length of the shortest path between nodes i and j of the N-node network [6]. The dependence of the GRT $\langle T_R \rangle$ of each network realization on its average path length ($\mathcal{L}$) is presented in figure 4(c). We observe that $\langle T_R \rangle$ exhibits a negative correlation coefficient of -0.658 with respect to $\mathcal{L}$, i.e., random scale-free networks with shorter characteristic path lengths synchronize slower. This result is compatible with the fact that random scale-free networks with longer characteristic path lengths have been previously shown to promote synchronizability [28]. The underlying heuristic picture is that a small $\mathcal{L}$ in such networks corresponds to a large amount of traffic passing through the few 'central' nodes connected to each other which facilitate communication between the much larger population of the other oscillators. This may lead to destructive interference of the different signals passing through such nodes. Subsequently, there may not be significant overall communication between the different oscillators of the network, thereby culminating in its reduced synchronizability [28].

3.3. Power grid of the United Kingdom

As a final more realistic example, we consider a conceptual model of the power transmission grid of the United Kingdom with second-order Kuramoto-type nodal dynamics [43]. The network consists of $N = 120$ nodes and 165 transmission lines (as illustrated in figure 5) with topological properties much different from those of a scale-free network. The dynamical equations of the system (in analogy with equation (1)) read [10]

$$\dot{\theta}_i = \omega_i,$$
$$\dot{\omega}_i = -\alpha\omega_i + P_i + \epsilon \sum_{j=1}^{N} A_{ij} \sin(\theta_j - \theta_i), \tag{9}$$

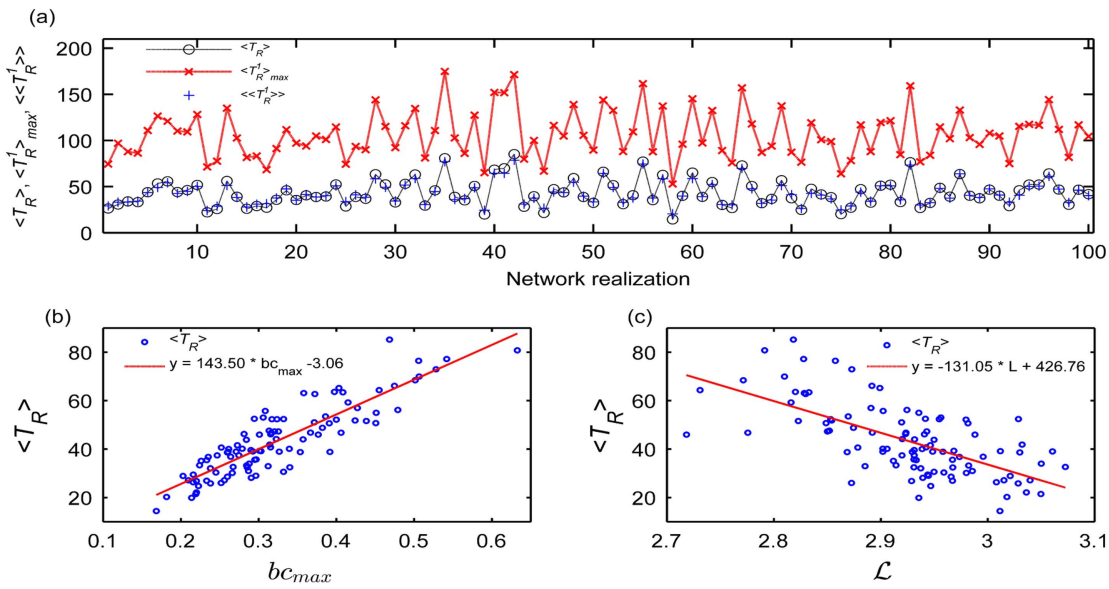

Figure 4. (a) Global RT $\langle T_R \rangle$ (black circles), maximum SNRT $\langle T_R^1 \rangle_{\max}$ (red crosses) and average SNRT $\langle\langle T_R^1 \rangle\rangle$ (blue crosses) of all network realizations from the considered ensemble of random scale-free networks. (b) Relationship between $\langle T_R \rangle$ (blue circles) and the maximum betweenness centrality ($bc_{\max}$) of all nodes of the respective network realization. (c) As in (b) for $\langle T_R \rangle$ and average path length ($\mathcal{L}$) of the respective network realization. The red lines in (b), (c) indicate linear fits.

where θ_i, ω_i, α and P_i denote the phase, frequency, electromechanical damping constant and net power input of the ith oscillator, respectively. Furthermore, we randomly choose $\frac{N}{2}$ net generators and $\frac{N}{2}$ net consumers with $P_i = +P_0$ and $P_i = -P_0$, respectively [8]. We use the parameter values of $\alpha = 0.1$, $P_0 = 1.0$ and $\epsilon = 9.0$ for obtaining the results described below.

We again consider the synchronized state, which corresponds to all oscillators having constant phases $\tilde{\theta}^i$ and frequencies $\tilde{\omega}^i = 0$, as the DOS of the grid. We select $I_C = 1000$ trials for calculating the SNRT values of the network. The $\langle T_R^1 \rangle$ values (for $\delta = 10^{-4}$) of all the $N = 120$ nodes are shown in figures 6(a) and (b) displays a histogram of all $\langle T_R^1 \rangle$ values. Interestingly, we observe from figures 6(a), (b) that 113 nodes have low values of SNRT ($\langle T_R^1 \rangle \leqslant 200$), which are shown in black in figure 6. However, we also observe seven *slow* nodes that exhibit substantially higher values ($\langle T_R^1 \rangle > 200$), which are marked in red in figure 6. Therefore, (individually or collectively) perturbing any of these seven nodes of the network will result in dysfunction of the grid and a significantly longer time until the system retaliates to the synchronized state. In turn, it is recommended to control or safeguard these seven specific nodes of the network to avoid a long waiting time for the system to return to the synchronized state in the face of random perturbations. The choice of the boundary at $\langle T_R^1 \rangle = 200$ for distinguishing between the *fast* and *slow* nodes is motivated by the fact that we observe a first substantial gap in the histogram in figure 6(b) around the aforementioned value. We also find similar results from a cluster analysis of the $\langle T_R^1 \rangle$ values of the network. These seven nodes are not found to exhibit any specific topological features leading to their relatively higher respective $\langle T_R^1 \rangle$ values. Further investigations analysing these results may provide potentially important insights in this regard.

We emphasize that Erdős–Rényi random networks [6] of Rössler oscillators are found to exhibit similar distributions of $\langle T_R^1 \rangle$ values as above; the corresponding results are described in appendix D. Figures 6(c), (d) illustrates the values of $\langle T_R^1 \rangle$ in comparison with k and bc, respectively. The correlation coefficients of $\langle T_R^1 \rangle$ with k and bc are 0.102 and 0.061, respectively, ruling out the existence of a systematic dependence between $\langle T_R^1 \rangle$ and k or bc. Figure 5 displays the network topology together with the individual $\langle T_R^1 \rangle$ values in analogy with figure 2 for the DSF network of Rössler oscillators.

4. Conclusions

Complex systems modelled as networks of interacting dynamical units are ubiquitous and often exhibit multiple stable states. Maintaining operation of such systems in the desired stable state (which often concurs with the synchronized state of the network) is vital to their functionality. Subsequently, this has generated a lot of attention in studying stability of the DOS in such coupled dynamical systems. However, given that the DOS is

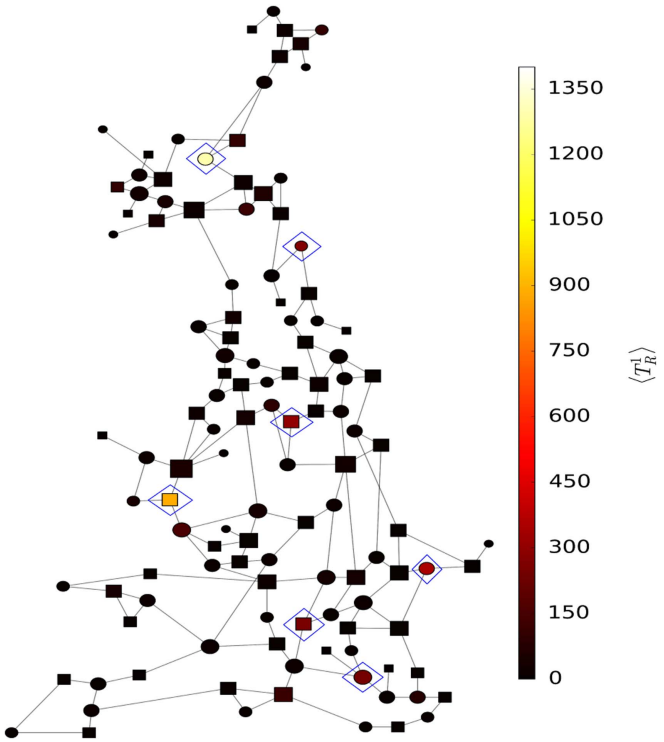

Figure 5. Network topology of the power transmission grid of the United Kingdom (comprising $N = 120$ nodes) with second-order Kuramoto-type nodal dynamics. Circular nodes denote net generators while square nodes are net consumers. The size of each symbol is proportional to the degree, and its colour corresponds to the $\langle T_R^1 \rangle$ value of the respective node. The seven nodes further encircled by blue diamonds comprise the *slow* nodes of the grid in our simplified model.

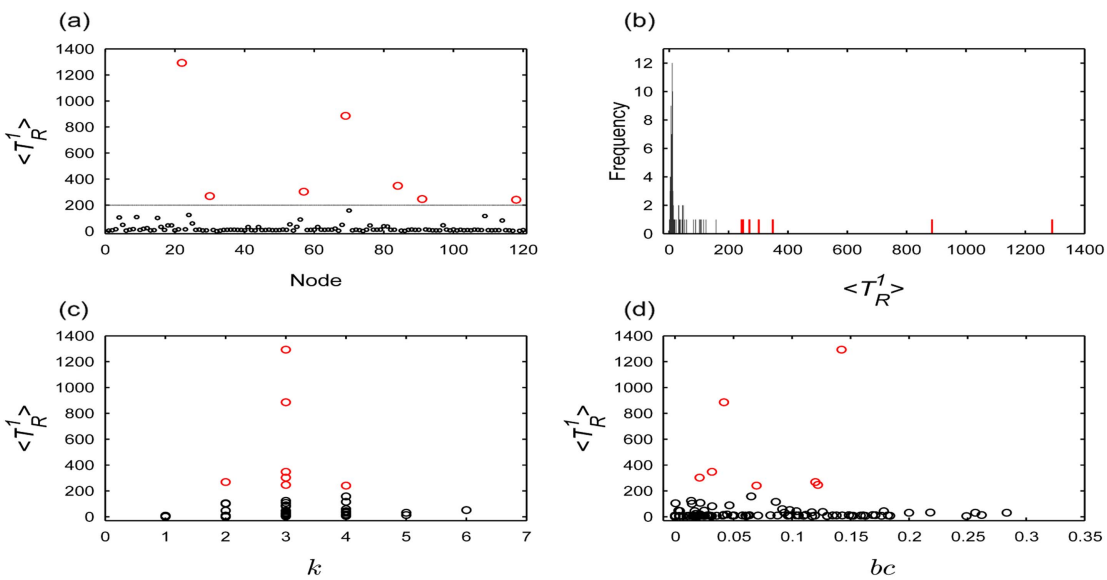

Figure 6. (a) SNRT $\langle T_R^1 \rangle$ of all the $N = 120$ nodes of the power grid of the United Kingdom with second-order Kuramoto-type nodal dynamics. (b) Histogram of $\langle T_R^1 \rangle$ of all the $N = 120$ nodes. (c), (d) Dependence of $\langle T_R^1 \rangle$ on (c) degree (k) and (d) betweenness centrality (bc) of the nodes. The *fast* nodes of the grid with $\langle T_R^1 \rangle \leqslant 200$ are shown in black while the *slow* nodes having $\langle T_R^1 \rangle > 200$ are marked in red.

stable in principle, it is equally important that the system relaxes back to the same as quickly as possible, following a random perturbation to a particular node of the network. We have addressed this issue here by proposing the general framework of SNRT which relates to the time taken by the system operating in the DOS to return to the same, following a non-infinitesimal perturbation to the dynamical state of the respective node. It is

important to note that we did not address the problem of driving the perturbed system to the DOS. Instead, we aimed at unveiling the different relative time scales underlying the transient dynamics of individual nodes of the network during its relaxation to the DOS, in order to identify specific nodes which when perturbed lead to significantly enlarged RT. We thus recommend taking precautionary measures of safeguarding primarily these nodes of the network from external perturbations.

Importantly, the proposed machinery can be utilized in revealing relationships between topological features of nodes and their respective SNRT values and in turn, the GRT of the overall network. Further, we have suggested the association of SNRT with the concept of engineering resilience in quantifying the resilience of such networked dynamical systems. Finally, we have applied the framework of SNRT to deterministic and random scale-free networks of Rössler oscillators and a conceptual model of the power grid of the United Kingdom with second-order Kuramoto-type nodal dynamics.

We have presented here the framework of SNRT (and associated illustrations) in the special context of networks of identical oscillators with continuous time dynamics (equation (1)) exhibiting bistability on account of coexisting synchronized and desynchronized regimes. However, the framework is generally applicable to any networked (continuous or discrete time) dynamical system with non-identical nodes and multiple coexisting states. Thus, future work on SNRT could comprise its extension and application to networks of non-identical nodes and/or exhibiting more complex patterns of multistability. Further development on SNRT could comprise its generalization to a framework of *multiple-node recovery time*, similar to recent work in the context of BS [10].

Regarding a potential field of application, we emphasize that time-delays arise frequently in the inherent dynamics of individual oscillators and in their interactions on complex networks [44]. Therefore, another interesting endeavour could constitute incorporating time-delays in networked dynamical systems and investigating their influence on SNRT and GRT of the network. Finally, complex systems comprising oscillators coupled on prototypical network types such as Watts–Strogatz, multilayer, interdependent, etc are open to applications of SNRT. These ventures could further unravel interesting relationships between SNRT and topological features of the aforementioned networks.

Acknowledgments

CM and RVD have been supported by the German Federal Ministry of Education and Research (BMBF) via the Young Investigators Group CoSy-CC^2 (grant no. 01LN1306A). TK, JK and RVD acknowledge support from the IRTG 1740/TRP 2011/50151-0, funded by the DFG/FAPESP. The authors gratefully acknowledge the European Regional Development Fund (ERDF), the German Federal Ministry of Education and Research (BMBF) and the Land Brandenburg for supporting this project by providing resources on the high performance computer system at the Potsdam Institute for Climate Impact Research.

Appendix A. On the choice of the reference trajectory

We elaborate here on the existence of a reference state such that the condition in equation (4) is fulfilled. For any arbitrary $\mathbf{x}_{\mathrm{ref}}$ we have the corresponding T_{RR} function, and hence $\langle T_R^1(i)\rangle$ as well. Now, we can take a new $\mathbf{x}'_{\mathrm{ref}} = \varphi(-t, \mathbf{x}_{\mathrm{ref}})$ where $\varphi(-t, \cdot)$ is the time-evolution operator shifting a state for the time t backwards along the flow and $t = \langle T_R^1\rangle_{\min}$. Using $\mathbf{x}'_{\mathrm{ref}}$ we have a corresponding T'_{RR} function and $\langle T_R^{1'}(i)\rangle$. In particular, $\langle T_R^{1'}\rangle_{\min} = 0$ holds by construction. So, taking $\mathbf{x}'_{\mathrm{ref}}$ as the reference state fulfils equation (4).

Appendix B. DSF network

The DSF network was proposed by Barabási *et al* [39] as a simple model to generate scale-free topologies in a deterministic fashion with hierarchical assembly. It was later analytically studied by Iguchi and Yamada [45] in greater detail. Such networks characterized by their fractal growth are categorized into the general class of hierarchical networks [46].

The construction of the network follows an iterative rule which starts with a single vertex labelled as the *root* node of the network. Subsequently, two nodes labelled as *bottom* nodes are added and connected to the root, thus completing the 1st step of the construction process. Then, two identical copies of the resulting graph are created and each of the bottom nodes of these two units are connected to the root in the 2nd step. Thus, the root gains four more edges and the resulting network now contains nine nodes. In the 3rd step, two copies of the resulting graph are created, and the eight bottom nodes of each of these 2 units are connected to the root.

Generalizing the aforementioned steps to the nth iteration would involve adding two units of $3^n - 1$ nodes created in the $(n-1)$th step and then connecting the 2^n bottom nodes of each unit to the root node. We refer to each step of the algorithm as a *generation*. The topology developed over three generations of the DSF network is illustrated in figure 1.

The degree distribution of the network can be exactly solved for and follows $P(k) \sim k^{-\frac{3}{2}}$ [39]. Also, the average path length of such a network developed over g generations can be analytically obtained to be $\mathcal{L} = \frac{8g3^{g-2}}{3^g - 1}$, which in the limit of $N \to \infty$ is approximated by $\frac{8}{9\log 3}\log N$ [47]. Thus, the average path length scales logarithmically with the number of nodes for large DSF networks [39].

The *local clustering coefficient* $\mathcal{C}_i^{\mathrm{L}}$ is a measure of the probability of the existence of a link between two randomly selected neighbours of node i [6]. $\mathcal{C}_i^{\mathrm{L}}$ is defined as the ratio between the number of links between vertices within the neighbourhood of node i and the number of links that could possibly exist between them [6]. Thus, $\mathcal{C}_i^{\mathrm{L}} = \frac{2}{k_i(k_i-1)}N_i^{\Delta}$ where N_i^{Δ} is the total number of closed triangles including node i (with degree k_i), which is bounded by the maximum possible value of $\frac{k_i(k_i-1)}{2}$ [6]. The *average local clustering coefficient* $\mathcal{C}^{\mathrm{L}}$ of the network is then given by the arithmetic mean of the local clustering coefficient of all nodes of the network, i.e., $\mathcal{C}^{\mathrm{L}} = \frac{1}{N}\sum_{i=1}^{N}\mathcal{C}_i^{\mathrm{L}}$. The DSF network model does not involve creation of triangles of nodes, thereby resulting in no clustering, i.e, an average clustering coefficient of $\mathcal{C}^{\mathrm{L}} = 0$ [39].

Appendix C. BA model of random scale-free networks

Many real-world complex networks have been reported to exhibit scale-free behaviour characterized by the probability $P(k)$ that a randomly selected node has exactly k links decaying as a power law, $P(k) \sim k^{-\gamma}$, where $2 < \gamma < 3$ has been typically observed for the scaling exponent γ [41]. This leads to a heterogeneous degree distribution in such scale-free networks with mostly low degree nodes coexisting with a few very high degree nodes (also called *hubs*) [41].

In the above context, the BA model [41] has been suggested for realizing random scale-free networks with growth and preferential attachment, where an incoming node is more likely to get randomly linked to an existing node with higher connectivity. While generating the random scale-free networks using the BA model, the growing character of the network is incorporated by starting with a small number of connected nodes N_0 with uniform degree. Thereafter, at every time step a new node is introduced and linked to m nodes already present in the system (until the network comprises N nodes). We set $N_0 = 3$ and $m = 2$ for generating the ensemble of random scale-free networks considered in this paper (section 3.2). Preferential attachment is incorporated by assuming that the probability Π_i that a new node will be connected to an existing node i depends on the degree k_i of node i, such that $\Pi_i = \frac{k_i}{\sum_j k_j}$. This naturally creates the possibility of high degree nodes to continuously further increase their respective degrees, as new nodes added to the network prefer attachment with such hubs. The degree distribution in such a network indeed follows a power-law with $\gamma = 3$ while the average path length and average local clustering coefficient scale with network size as $\mathcal{L} \sim \frac{\log N}{\log\log N}$ and $\mathcal{C}^{\mathrm{L}} \sim \frac{(\log N)^2}{N}$, respectively [2, 48]. Such random scale-free networks generated using the BA model generally exhibit shorter average path lengths as well as higher values of clustering coefficients. However, the BA model fails to capture high levels of clustering exhibited by many real-world complex networks.

Appendix D. Erdős–Rényi random networks of Rössler oscillators

We consider an ensemble of 100 Erdős–Rényi random networks [6] of $N = 81$ Rössler oscillators each, again with the same parameter values as for the DSF network (section 3.1). We consider a probability $p = 0.04$ of a connection between any pair of vertices of a network, resulting in a total of 130 edges in each realization. For $\delta = 10^{-6}$, we calculate and present the distribution of $\langle T_R^1 \rangle$ (on $\log_{10}$ scale) values of all nodes of the considered ensemble of Erdős–Rényi random networks in figure D1. It is evident from the distribution that most nodes have rather low values of $\langle T_R^1 \rangle$ ($\leqslant 100$), which comprise the *fast* nodes of the respective network. However, we also observe the existence of very few *slow* nodes which exhibit much higher $\langle T_R^1 \rangle$ (> 100) values. The $\langle T_R^1 \rangle$ values again do not exhibit any strong linear relationship with k (bc), (not shown) as demonstrated by the correlation coefficient of 0.743 (0.36).

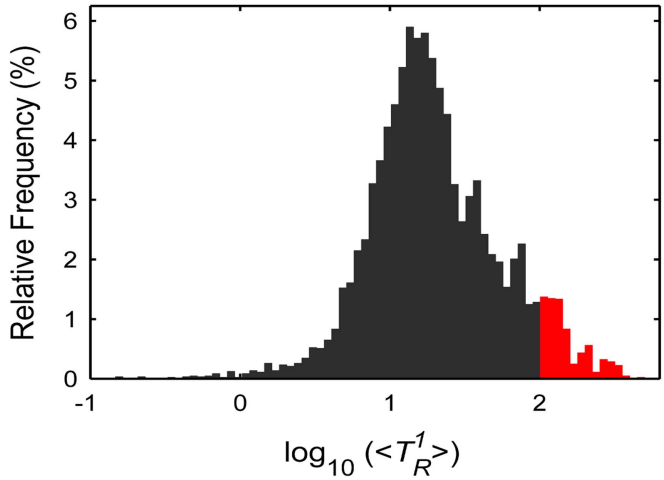

Figure D1. Distribution of SNRT $\langle T_R^1 \rangle$ (on $\log_{10}$ scale) of all nodes of the considered ensemble of Erdős–Rényi random networks. The relative frequencies (%) correspond to the percentage of nodes with $\log_{10}(\langle T_R^1 \rangle)$ values lying within the respective bin. The *fast* nodes of the ensemble with $\langle T_R^1 \rangle \leqslant 100$ are shown in black while the *slow* nodes having $\langle T_R^1 \rangle > 100$ are marked in red.

References

[1] Strogatz S H 2001 Exploring complex networks *Nature* **410** 268–76
[2] Albert R and Barabási A-L 2002 Statistical mechanics of complex networks *Rev. Mod. Phys.* **74** 47
[3] Dorogovtsev S N and Mendes J F F 2002 Evolution of networks *Adv. Phys.* **51** 1079–187
[4] Newman M E J 2003 The structure and function of complex networks *SIAM Rev.* **45** 167–256
[5] Boccaletti S, Latora V, Moreno Y, Chavez M and Hwang D-U 2006 Complex networks: structure and dynamics *Phys. Rep.* **424** 175–308
[6] Newman M 2010 *Networks: An Introduction* (New York: Oxford University Press)
[7] Pikovsky A, Rosenblum M and Kurths J 2003 *Synchronization: A Universal Concept in Nonlinear Sciences* vol 12 (Cambridge: Cambridge University Press)
[8] Menck P J, Heitzig J, Kurths J and Schellnhuber H J 2014 How dead ends undermine power grid stability *Nat. Commun.* **5** 3969
[9] Menck P J, Heitzig J, Marwan N and Kurths J 2013 How basin stability complements the linear-stability paradigm *Nat. Phys.* **9** 89–92
[10] Mitra C, Choudhary A, Sinha S, Kurths J and Donner R V 2017 Multiple-node basin stability in complex dynamical networks *Phys. Rev.* E **95** 032317
[11] Arenas A, Díaz-Guilera A, Kurths J, Moreno Y and Zhou C 2008 Synchronization in complex networks *Phys. Rep.* **469** 93–153
[12] Pecora L M and Carroll T L 1998 Master stability functions for synchronized coupled systems *Phys. Rev. Lett.* **80** 2109
[13] Hellmann F, Schultz P, Grabow C, Heitzig J and Kurths J 2016 Survivability of deterministic dynamical systems *Sci. Rep.* **6** 29654
[14] Zumdieck A, Timme M, Geisel T and Wolf F 2004 Long chaotic transients in complex networks *Phys. Rev. Lett.* **93** 244103
[15] Timme M, Wolf F and Geisel T 2004 Topological speed limits to network synchronization *Phys. Rev. Lett.* **92** 074101
[16] Timme M, Geisel T and Wolf F 2006 Speed of synchronization in complex networks of neural oscillators: analytic results based on random matrix theory *Chaos* **16** 015108
[17] Qi G X, Huang H B, Chen L, Wang H J and Shen C K 2008 Fast synchronization in neuronal networks *Europhys. Lett.* **82** 38003
[18] Qi G X, Huang H B, Shen C K, Wang H J and Chen L 2008 Predicting the synchronization time in coupled-map networks *Phys. Rev.* E **77** 056205
[19] Son S-W, Jeong H and Hong H 2008 Relaxation of synchronization on complex networks *Phys. Rev.* E **78** 016106
[20] Zillmer R, Brunel N and Hansel D 2009 Very long transients, irregular firing, and chaotic dynamics in networks of randomly connected inhibitory integrate-and-fire neurons *Phys. Rev.* E **79** 031909
[21] Granada A E and Herzel H 2009 How to achieve fast entrainment? The timescale to synchronization *PLoS One* **4** e7057
[22] Grabow C, Hill S M, Grosskinsky S and Timme M 2010 Do small worlds synchronize fastest? *Europhys. Lett.* **90** 48002
[23] Grabow C, Grosskinsky S and Timme M 2011 Speed of complex network synchronization *Eur. Phys. J.* B **84** 613–26
[24] Wang S-J, Du R-H, Jin T, Wu X-S and Qu S-X 2016 Synchronous slowing down in coupled logistic maps via random network topology *Sci. Rep.* **6** 23448
[25] Kittel T, Heitzig J, Webster K and Kurths J 2017 Timing of transients: quantifying reaching times and transient behavior in complex systems *New J. Phys.* **19** 083005
[26] Fries P 2005 A mechanism for cognitive dynamics: neuronal communication through neuronal coherence *Trends Cogn. Sci.* **9** 474–80
[27] Fell J and Axmacher N 2011 The role of phase synchronization in memory processes *Nat. Rev. Neurosci.* **12** 105–18
[28] Nishikawa T, Motter A E, Lai Y-C and Hoppensteadt F C 2003 Heterogeneity in oscillator networks: are smaller worlds easier to synchronize? *Phys. Rev. Lett.* **91** 014101
[29] Watts D J and Strogatz S H 1998 Collective dynamics of 'small-world' networks *Nature* **393** 440–2
[30] Barahona M and Pecora L M 2002 Synchronization in small-world systems *Phys. Rev. Lett.* **89** 054101
[31] Holling C S 1973 Resilience and stability of ecological systems *Annu. Rev. Ecol. Systematics* **4** 1–23
[32] Holling C S 1996 Engineering resilience versus ecological resilience *Engineering Within Ecological Constraints* (Washington, DC: National Academy Press) (https://doi.org/10.17226/4919)
[33] Pimm S L 1984 The complexity and stability of ecosystems *Nature* **307** 321–6
[34] Gunderson L H 2000 Ecological resilience-in theory and application *Annu. Rev. Ecol. Systematics* **31** 425–39

[35] Mitra C, Kurths J and Donner R V 2015 An integrative quantifier of multistability in complex systems based on ecological resilience *Sci. Rep.* **5** 16196
[36] Walker B, Holling C S, Carpenter S R and Kinzig A 2004 Resilience, adaptability and transformability in social-ecological systems *Ecol. Soc.* **9** 5
[37] Gunderson L H, Allen C R and Holling C S 2012 *Foundations of Ecological Resilience* (Washington, DC: Island Press) (https://doi.org/10.1086/663884)
[38] Rössler O E 1976 An equation for continuous chaos *Phys. Lett.* A **57** 397–8
[39] Barabási A-L, Ravasz E and Vicsek T 2001 Deterministic scale-free networks *Physica* A **299** 559–64
[40] Huang L, Chen Q, Lai Y-C and Pecora L M 2009 Generic behavior of master-stability functions in coupled nonlinear dynamical systems *Phys. Rev.* E **80** 036204
[41] Barabási A-L and Albert R 1999 Emergence of scaling in random networks *Science* **286** 509–12
[42] Holme P, Kim B J, Yoon C N and Han S K 2002 Attack vulnerability of complex networks *Phys. Rev.* E **65** 056109
[43] Rodrigues F A, Peron T K D M, Ji P and Kurths J 2016 The kuramoto model in complex networks *Phys. Rep.* **610** 1–98
[44] Mitra C, Ambika G and Banerjee S 2014 Dynamical behaviors in time-delay systems with delayed feedback and digitized coupling *Chaos Solitons Fractals* **69** 188–200
[45] Iguchi K and Yamada H 2005 Exactly solvable scale-free network model *Phys. Rev.* E **71** 036144
[46] Ravasz E and Barabási A-L 2003 Hierarchical organization in complex networks *Phys. Rev.* E **67** 026112
[47] Zhang Z, Lin Y, Gao S, Zhou S and Guan J 2009 Average distance in a hierarchical scale-free network: an exact solution *J. Stat. Mech.: Theory Exp.* **2009** P10022
[48] Bollobás B and Riordan O M 2003 Mathematical results on scale-free random graphs *Handbook of Graphs and Networks: From the Genome to the Internet* (Weinheim: Wiley-VCH) pp 1–34